Analysis of tunable photonic crystal directional couplers

Elissavet P. Kosmidou,[a] Emmanouil E. Kriezis,[b] and Theodoros D. Tsiboukis[c]
Applied and Computational Electromagnetics Laboratory, Department of Electrical and Computer Engineering, Aristotle University of Thessaloniki, GR-54124 Thessaloniki, Greece

(Received 10 January 2006; accepted 14 July 2006; published online 31 August 2006)

Tunable directional coupler structures based on triangular photonic crystal lattices are investigated using the finite difference time domain method. The infiltration of nematic liquid crystal materials into the coupler waveguides allows for the control of its properties through the application of external static electric fields, which reorient the nematic director. Strong dynamical shifting of the dispersion curves, along with the decoupling frequencies and the coupling coefficient, is demonstrated. Such features render this class of couplers suitable for a range of applications. The coupling lengths accomplished are quite short even when the interaction region between the two coupler branches is widened. Furthermore, operation as a channel interleaver in wavelength division multiplexing systems is explored, and it is revealed that by proper selection of the geometrical parameters a constant channel separation of 0.8 nm is achieved, with an overall length of a few hundreds of microns in wide frequency ranges. © *2006 American Institute of Physics*.
[DOI: 10.1063/1.2335800]

I. INTRODUCTION

Directional couplers are basic components in optical systems, where they are primarily used as power splitters, wavelength selective filters, switches, modulators, channel interleavers, or multiplexers-demultiplexers (MUXs-DEMUXs). Recently, there have been reported various directional coupler configurations based on photonic crystal lattices.[1,2] This trend is due to the fact that photonic crystal couplers offer substantially shorter beat lengths compared to the conventional ones, allowing for devices of very short lengths which are suitable for integration in ultracompact optical circuits. It has been already shown that a grating with a long period and small properly chosen amplitude can strengthen the coupling properties, when placed between the waveguides.[3]

Since then, a variety of photonic crystal directional couplers and optical devices founded on them have been theoretically and experimentally studied. The square lattice of dielectric rods was used to design directional couplers which can achieve channel spacings of 0.8 and 20 nm with drastically reduced sizes, and based on them two- and four-channel MUX-DEMUX were presented.[4] Furthermore, the coupling characteristics of two closely spaced straight photonic crystal waveguides and their ability to operate as channel interleavers in wavelength division multiplexing (WDM) systems were investigated and it was also proven that the appropriate defective geometry in the interaction area can result in the decoupling of the waveguides.[5] This property is quite significant, since it predicts the lack of mutual interference (crosstalk) between adjacent waveguides and permits highly integrated optical circuits to be built. The conditions for decoupling of waveguides formed in a periodic square lattice of dielectric rods have been analyzed and found to directly depend on the symmetry of the geometry.[6] Moreover, a method for the reduction of the coupling length in photonic crystal directional couplers was proposed.[7] This approach was based on diminishing the effective dielectric constant of the region interceding between the waveguides. It was indeed demonstrated that the coupling coefficient, as well as its slope, are increased, and a 0.8 nm channel interleaver with a total length smaller than 200 μm was designed.

The triangular lattice of air holes drilled into a semiconductor slab, which provides confinement in the vertical direction and is more suitable for integration with optoelectronic components, has been also studied as a cladding for directional couplers. In this case too, a 200 μm long directional coupler was shown to operate as a WDM channel interleaver with 0.8 nm spacing at 1.5 μm and wavelength demultiplexing at 1.31/1.55 μm in a device as short as 2 μm was obtained, exploiting the waveguide decoupling.[8] Furthermore, the idea of contradirectional coupling between waveguides formed in a triangular lattice was used to design add-drop filter configurations characterized by reduced losses.[9] Additionally, the waveguide decoupling in triangular lattices of dielectric rods was analyzed, along with a compact dual wavelength demultiplexer in which a loop-shaped waveguide is adapted at the output port to improve the output power ratio.[10]

Moreover, directional couplers based on perforated slabs have been constructed and experimentally measured.[11,12] In addition to that, many optical circuit elements possessing attractive characteristics have been designed on photonic crystal directional couplers, such as compact notch-rejection filters[13] and power splitters.[14]

Recently there have been reported efforts towards the direction of designing tunable optical elements based on photonic crystal configurations, among which are directional couplers. This goal is mainly achieved by employing nonlinear or liquid crystal materials.[15] In the former instance aiming at designing all-optical switching structures, the nonlin-

[a]Electronic mail: elkosm@auth.gr
[b]Electronic mail: mkriezis@auth.gr
[c]Electronic mail: tsibukis@auth.gr

ear material was introduced into the region between the two branches of the coupler, and a control signal of appropriate power was used to alter the dielectric constant of the coupling area and therefore change the coupling characteristics.[16] Alternatively, the two waveguides were made of nonlinear material so that the power of the input signal determined whether the coupler operated in the bar/cross states or as a power splitter.[17] On the other hand, the change in the effective refractive index caused by the reorientation of liquid crystal molecules by means of an applied static electric field can likewise alter the operation of a directional coupler. This property has been exploited in various other devices such as photonic crystal cavities[18,19] and Y-shaped waveguides.[20] Furthermore, the coupling strength related to the input beam polarization and temperature was studied in a multiguide directional coupler with a gratinglike indium tin oxide (ITO) electrode on a planar nematic liquid crystal film.[21] Recently, the concept of nematic liquid crystal infiltration in photonic crystal directional couplers has been also investigated. In a representative study, the liquid crystal was infiltrated into the air voids of both the photonic crystal cladding and the waveguides, and an optical switch was designed exploiting the decoupling properties of the device,[22] whereas in an alternative design liquid crystal layers formed the two waveguides, and the nematic director orientation across them determined the coupler operation.[23]

In this paper we examine the tunable coupling properties of two photonic crystal directional coupler layouts, where nematic liquid crystal materials are infiltrated into the waveguiding regions only. All the calculations were conducted using an anisotropic form of the two-dimensional (2D) finite-difference time-domain (FDTD) method,[24,25] in combination with the appropriate periodic boundary conditions[26] and the material-independent perfectly matched layer (MI-PML) absorber.[27,28]

II. TUNABLE PHOTONIC CRYSTAL DIRECTIONAL COUPLERS

Directional couplers are systems of two waveguides in close proximity. Light waves travel periodically between the waveguides, and the necessary prerequisite for maximum coupling is synchronism (waveguide modes must have the same propagation constant). Practically, this means that the waveguides should be identical. For each mode of the single isolated waveguide, the directional coupler supports two supermodes, one of even and one of odd parity, with respect to the plane equidistant from the waveguides. The two supermodes are characterized by different propagation constants k_{even} and k_{odd}. Light injected in the system shifts periodically between the two waveguides. The period of this transfer is called beat length L_B and is defined as $L_B=2\pi/|k_{\text{even}}-k_{\text{odd}}|$, while the necessary distance for light to migrate from the one waveguide to the other is the coupling length $L_c=\pi/|k_{\text{even}}-k_{\text{odd}}|=L_B/2$. Another characteristic quantity defining the coupling strength of the waveguides is the coupling coefficient $\kappa=|k_{\text{even}}-k_{\text{odd}}|/2$. Therefore, a light wave launched into one of the waveguides is coupled entirely to the opposite (cross state) when the coupler length is an odd multiple of the coupling length and comes out through the input waveguide (bar state) when the coupler length is an integer multiple of the beat length. In this paper, we investigate the tunable coupling characteristics of two photonic crystal directional couplers where nematic liquid crystal materials are introduced into the waveguides. Two coupler layouts are studied: in the first the nematic liquid crystal is inserted into the air holes composing the two photonic crystal waveguides, while in the second each guiding core consists of a liquid crystal layer.

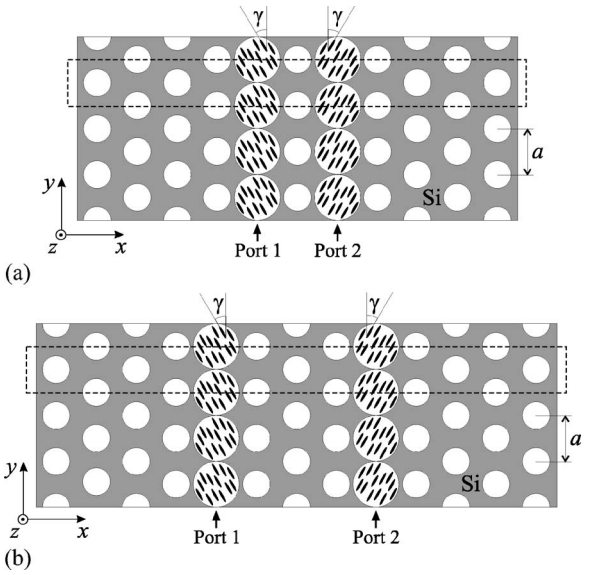

FIG. 1. Layout of directional couplers (a) I and (b) II. The dashed frame denotes the computational window.

A. Directional couplers I and II: Uniform planar director orientation inside the voids forming the waveguides

The first directional coupler configuration under study is depicted in Figs. 1(a) and 1(b). We shall refer to these two geometries as couplers I and II, respectively. They are designed on a triangular lattice of circular air voids drilled in silicon. The radius of each cylinder equals $0.3a$, where a is the photonic crystal lattice constant, while the relative permittivity of Si is 11.4. Such a photonic crystal possesses a wide band gap along the ΓK direction spanning from $0.2125(c/a)$ to $0.2972(c/a)$. Two identical straight parallel waveguides are formed by introducing two types of defects into the perfect periodic lattice. At first, the radius of the air voids in two rows along the ΓK direction is increased from $0.3a$ to $0.5a$. Furthermore, the specific two rows are shifted by $a/2$ along the vertical direction (y axis). This latter modification enhances the waveguide single mode propagation bandwidth[22] and thus the operational frequency range where the coupler supports only two supermodes of opposite parity, so that secondary coupling mechanisms are avoided. Increasing the radius of the infiltrated voids to $0.5a$ serves the same purpose. It should be noted that this bandwidth enhancement is achieved at the expense of a reduction in the coupling coefficient. However, very strong waveguide coupling is not always desirable, since it degrades the output power ratio. A typical nematic liquid crystal material, such as E7, is infil-

trated into the air voids forming the waveguides. Although selective liquid crystal infiltration has not been reported so far in planar photonic crystal devices, nevertheless is has been demonstrated in microstructured optical fibers.[29] The ordinary and extraordinary refractive indices of E7 are chosen as 1.49 and 1.66, respectively. Additionally, the case of no anchoring at the inner surface of the cylinders has been assumed, so that the molecular orientation can be considered uniform (but at an arbitrary angle) throughout their cross section. The uniform director profile is an ideal profile which may differ at a certain level from practical configurations formed under weak anchoring conditions. However, it is employed in order to examine the tunable operation of the analyzed directional couplers at its full extent, since it accounts for complete liquid crystal realignment in the voids' cross section. Furthermore, our study is concentrated on the examination of planar molecular profiles, as shown in Figs. 1(a) and 1(b). This specific choice is justified by two main reasons. Firstly, the selected triangular lattice of air voids manifests a wide band gap along the ΓK direction for transverse electric (TE) modes, which contains the operational frequencies of the proposed couplers. Therefore, in order to exploit the liquid crystal realignment to tune the analyzed structures, one needs to control the refractive indices presented in the plane of the electric field, i.e., the plane of periodicity (*xy* plane). Possible realignment out of this plane will affect the tunable performance of the directional couplers in a much weaker sense. The second reason is related to the fact that formation of nonplanar profiles is energetically favored in cylinders of large radii.[30] Specifically, in the practically realizable case of homeotropic molecular alignment planar director profiles are expected in cylinders of radii smaller than 500 nm. At the same time, the radius of the infiltrated voids in the proposed structures is clearly smaller, when operation at telecom optical frequencies is envisaged. Planar director configurations have been already observed in experimental studies,[31] where nematic materials are infiltrated into the cylindrical air holes of diameter 100 −200 nm in a triangular lattice.

We have studied two geometries where the waveguides are separated by one or three rows of air holes [Figs. 1(a) and 1(b), respectively]. We have firstly calculated in Fig. 2 the dispersion diagram of the single isolated waveguide for TE modes and for two limiting values of the tilt angle γ, which determines the orientation of the liquid crystal molecules. The numerical simulations are conducted by an anisotropic-FDTD technique at a supercell containing one period of the structure, such as the one indicated by the dashed rectangle frame shown in Fig. 1. Periodic boundary conditions are imposed at the upper and lower boundaries along the vertical direction, while the reflections at the right and left limits are minimized by a MI-PML absorber. The shaded regions indicate the extended states inside the defect-free photonic crystal. Although three modes are supported by the waveguide, it is evident that in a large portion of the band gap single mode propagation is allowed, which is furthermore sensibly affected by the nematic director orientation. This is also true for the supermodes of the directional couplers which are demonstrated in the dispersion diagrams of Figs. 3(a) and 3(b) for various values of the tilt angle. It can be observed that two supermodes resulting from the splitting of each mode of the isolated waveguide appear inside the band gap. The ones that we will study are indicated on the figures. Besides the strong tuning, we can also perceive that the waveguides are decoupled at a specific frequency, which is also tuned with the molecular orientation. In fact when the interacting region involves three lattice periods, two crossing points for each case are observed. Based on the previous remark, an optical switch could be designed where an external electric field would shift the operation of the coupler from decoupling to perfect coupling.[22] Also, such couplers could be used to design tunable add/drop filters. We should note, in addition, that the decoupling condition for the square lattice of dielectric rods[6] is not valid for the triangular lattice of air holes. Specifically, decoupling in triangular lattices of air holes is observed even when the waveguides are separated by an even number of lattice periods. In general, waveguide decoupling is a very significant property since it opens the possibility of constructing highly integrated optical circuits. Furthermore, the use of liquid crystals makes tunable operation possible.

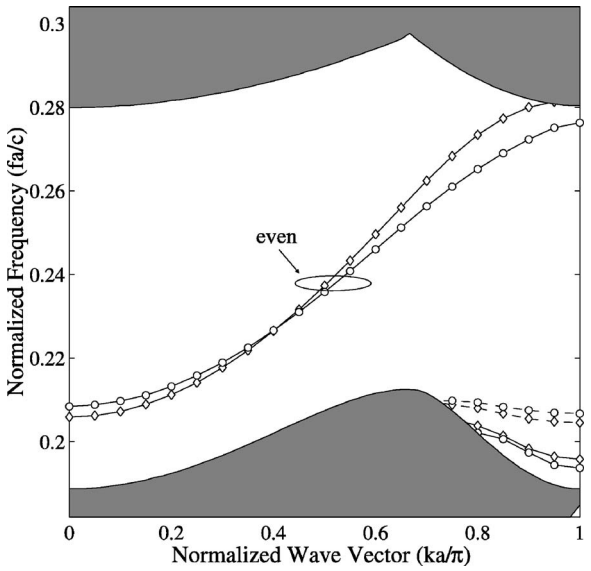

FIG. 2. Dispersion diagram for TE modes of the single isolated waveguide. Solid curves indicate even modes, and dashed curves correspond to odd modes. Diamonds: $\gamma=0°$; circles: $\gamma=90°$.

To further study the coupling strength of the waveguides, we compute the coupling lengths L_c and coupling coefficients κ of the directional couplers versus normalized frequency for the previously chosen values of the tilt angle. The results are plotted in Figs. 4(a) and 4(b) for coupler I and in Figs. 5(a) and 5(b) for coupler II. We present a frequency window which is common in the four cases and does not contain the decoupling points. Apart from the obvious tuning, it must be noticed that coupling lengths as short as two lattice constants are achieved in the first configuration, while the coupling length remains quite short, with a minimum value of approximately four lattice constants, even in the second instance where the region between the guiding arms is increased. This property predicts short lengths for potential application devices as well. In both occasions we can remark

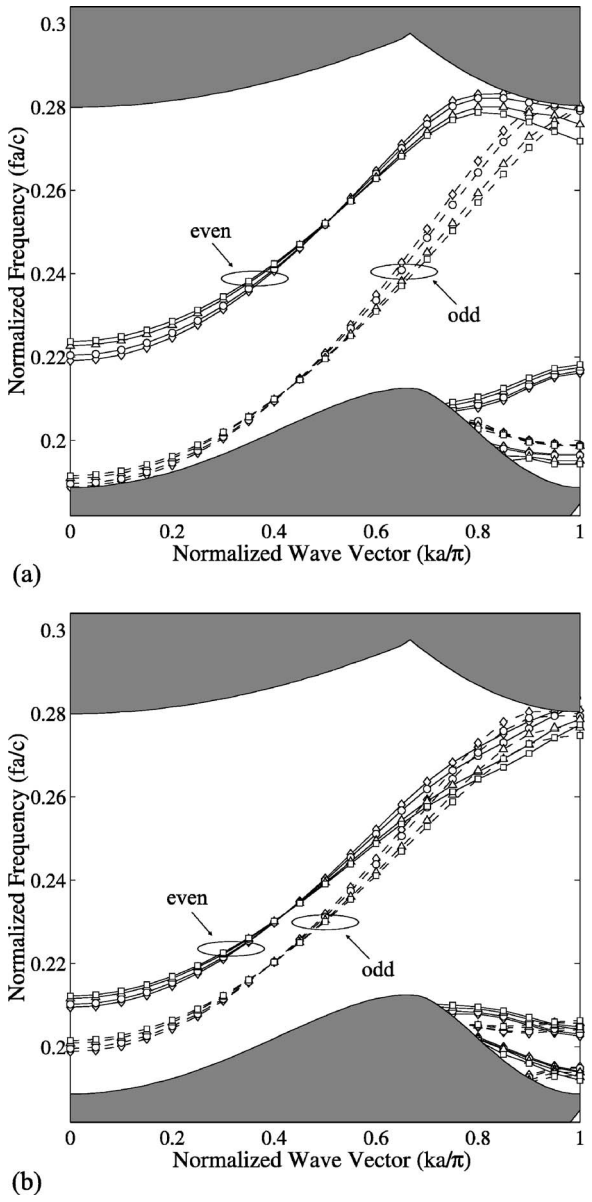

FIG. 3. Dispersion diagram for TE supermodes of directional couplers (a) I and (b) II. Solid curves indicate even supermodes, and dashed curves correspond to odd supermodes. Diamonds: $\gamma=0°$; circles: $\gamma=30°$; triangles: $\gamma=60°$; squares: $\gamma=90°$.

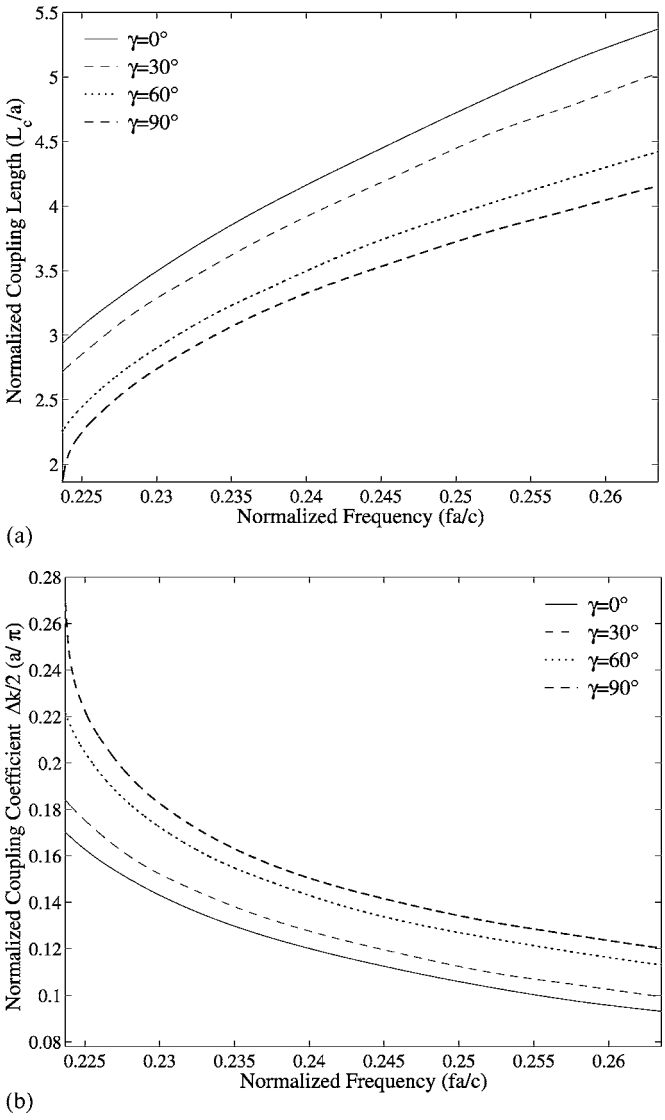

FIG. 4. (a) Normalized coupling length and (b) normalized coupling coefficient for different values of the tilt angle γ for directional coupler I.

that the coupling length is increased and as a consequence the coupling coefficient is reduced as the molecular orientation deviates from the horizontal position. The normalized power at the two coupler arms is shown in Figs. 6(a) and 6(b) for the two directional couplers. Both of them correspond to the case $\gamma=0°$, while the normalized operating frequency is set to $0.265(c/a)$ for coupler I and $0.23(c/a)$ for coupler II. Simulations are conducted by an anisotropic formulation of the FDTD algorithm, and the computational domain is terminated via the MI-PML absorbing boundary condition. Note that the periodic pattern of the photonic crystal is retained inside the absorbing layers in order to efficiently truncate the computational space. The power carried by each arm is calculated by integration of the Poynting vector at discrete points along the waveguide axis. The integration line for each port extends from the midpoint in the coupling region up to the limit of the computational space. The results for the coupling lengths are in complete agreement with the values derived from the dispersion diagrams. Moreover, the calculated power ratios between the two guiding arms are 9.7 dB for the first coupler and 15.26 dB for the second owing to the weaker coupling. The rippling in the graphs of Figs. 6(a) and 6(b) is expected due to the longitudinal profile of the supermodes, which naturally follows the periodicity of the photonic crystal cladding.

A preliminary study of coupler I has been conducted,[32] assuming strong homeotropic anchoring conditions at the surfaces of the guiding voids, which result in the formation of the more realistic planar-polar director profile.[30] The uniform profile analyzed so far is a limiting case of the planar-polar one when no anchoring is present and thus corresponds to the full tunable performance exhibited by these couplers. Initial results reported in Ref. 32 have indicated an imperceptible shift of the supermodes dispersion curves when studying the transition from no anchoring (uniform profile) to strong anchoring (planar polar profile) conditions. Maxi-

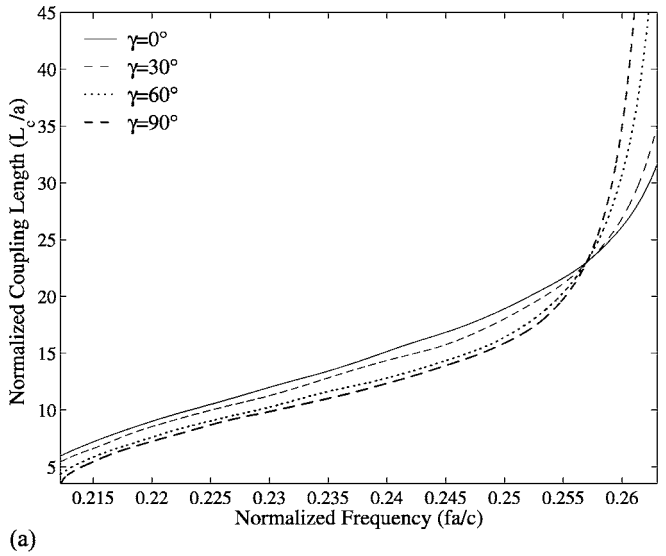

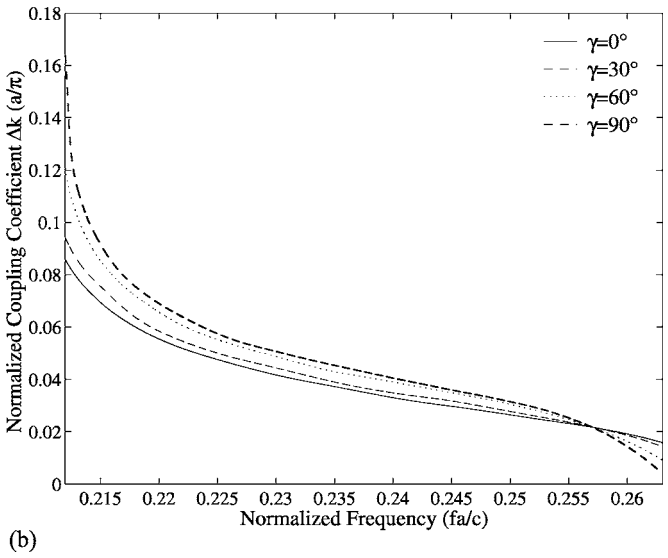

FIG. 5. (a) Normalized coupling length and (b) normalized coupling coefficient for different values of the tilt angle γ for directional coupler II.

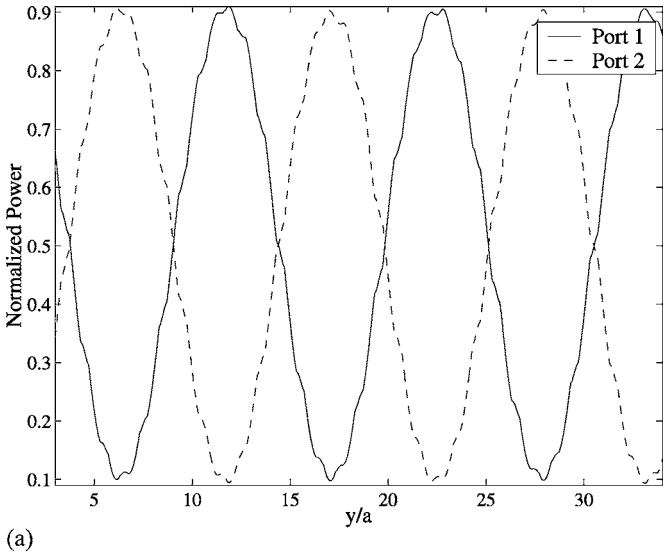

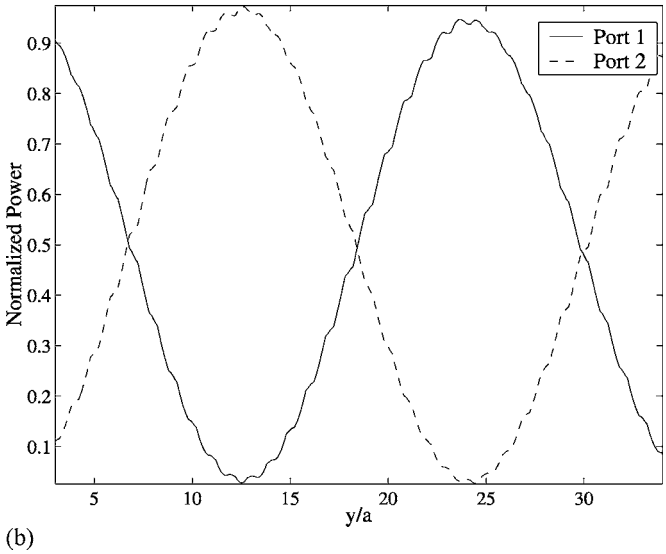

FIG. 6. Normalized power carried by each arm (a) of coupler I at frequency $0.265(c/a)$ and (b) of coupler II at frequency $0.23(c/a)$.

mum deviations in the coupling length between the previous two cases have been calculated to be around $0.2a$.

The capability of these couplers to operate as channel interleavers in WDM systems is investigated next. We have computed, using simple coupled mode theory,[33] the normalized output power at the two ports versus wavelength, so that we could find the appropriate coupler length in order to acquire desirable channel separations. We have naturally began by the case $\gamma=90°$, where the slope of the coupling coefficient curve is higher, and as a consequence narrower channel spacings are expected. An important factor taken into account is the attainment of wide wavelength windows where the coupling coefficient is linear and consequently the channel spacing is constant. Thus, the photonic crystal lattice period must be carefully chosen so that the operational wavelength range coincides with a section of the coupling coefficient curve where its slope is high and at the same time as constant as possible. Our results for coupler I are shown in Figs. 7(a) and 7(b). Figure 7(a) has been derived assuming that the lattice constant is $a=353$ nm and the length of the coupler as short as $L=550a=194.15$ μm. The wavelength spacing accomplished between adjacent channels is 0.8 nm, corresponding to 100 GHz grids, but due to the nonlinearity of the coupling coefficient this value is constant only in a narrow frequency window around 1550 nm. On the other hand [Fig. 7(b)], for $a=366$ nm and $L=1500a=549$ μm a constant channel separation of 0.8 nm is found in a wider range which covers a significant portion of the C band. Clearly, there is a trade-off between the coupler length and the linear-κ range (constant channel spacing). In addition, we can observe that for smaller values of γ the overall length required to achieve the same channel spacing is higher due to the lower slope of the coupling coefficient curve. Equivalently, the previous device length would lead to greater distances between consecutive channels. For example, when $\gamma=0°$ for $a=353$ nm and $L=194.15$ μm the channel separation in the C band varies from 1.4 to 1.9 nm, while for $a=366$ nm and $L=549$ μm the corresponding value is in the range of 0.9–1.2 nm. Evidently, the proposed coupler could be used in place of multiple couplers with different fixed

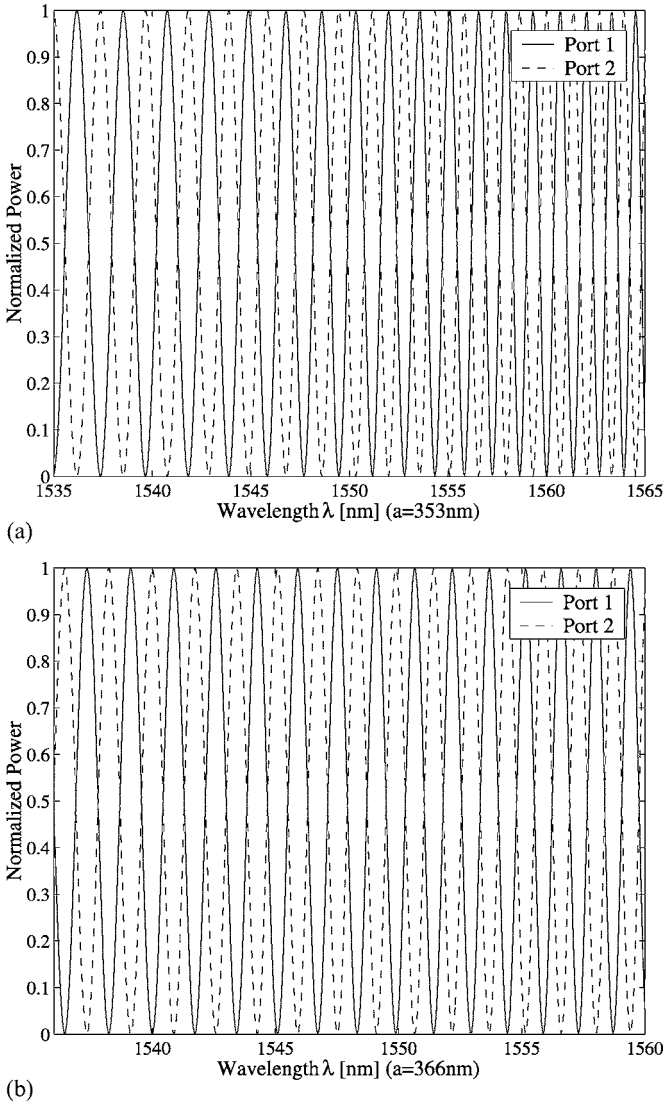

FIG. 7. Normalized power at the two output ports of coupler I for $\gamma=90°$ and (a) $L=550a=194.15$ μm, (b) $L=1500a=549$ μm.

properties, since its characteristics can be dynamically altered. Thus, the same coupler could be used in a number of stages of an either dense or coarse WDM system.

In Fig. 8 we have additionally calculated versus wavelength the relative phase shift of the two supermodes accumulated after propagating 1500 lattice constants, when the period of the photonic crystal lattice is $a=366$ nm. We can measure in the range of 1529.75–1569.59 nm (C band) for $\gamma=0°$ approximately 19 different wavelengths where the relative phase shift is an odd multiple of π, which suggests complete energy transfer from Port 1 to Port 2 (cross state), and another 19 wavelengths in between where the relative phase shift equals an even multiple of π, implying that the output energy is directed in Port 1 (bar state). Consequently, there are 38 narrow channels for the cross and bar states in total. The overall number of channels is increased to 50 when $\gamma=90°$ and it should be reminded that in a quite wide range within the C band the channels are equally spaced. Besides, it is obvious in Fig. 8 that the selected value of the lattice constant shifts the C band in almost linear regions on the coupling coefficient curves.

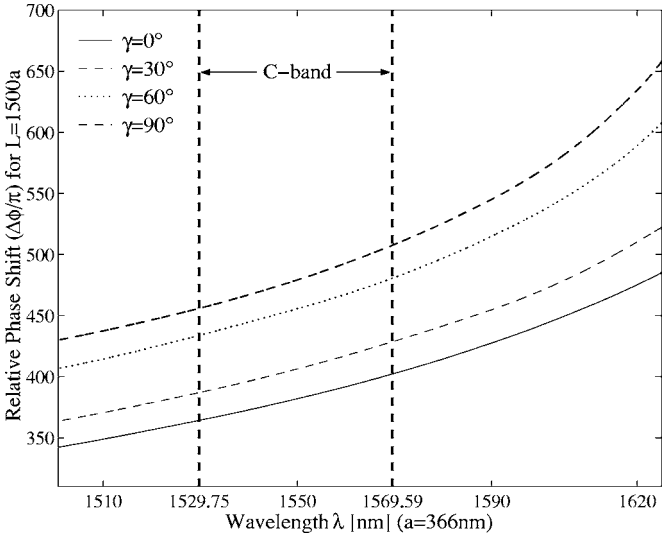

FIG. 8. Relative phase shift between the coupler I supermodes accumulated after $1500a$ when $a=366$ nm.

We have followed the previous procedure for coupler II as well. We have found that for $\gamma=90°$ when $a=335.5$ nm and $L=1400a=469.7$ μm, a constant channel spacing of 0.8 nm is achieved in a rather narrow range, which can be further enhanced by more appropriate selection of the lattice constant and coupler length. Naturally, the operation can be completely changed by reorienting the liquid crystal molecules. The normalized power at the two output ports is shown in Fig. 9, with the relative phase shift accumulated being depicted in Fig. 10. As it can be noticed, the specific choice of the lattice period shifts the C band in regions where the slope of the κ curve is high but not constant.

B. Directional coupler III: Liquid crystal layers as waveguides

The layout of the second directional coupler under investigation is depicted in Fig. 11. The photonic crystal cladding is the same as the one used in the previous section. The two

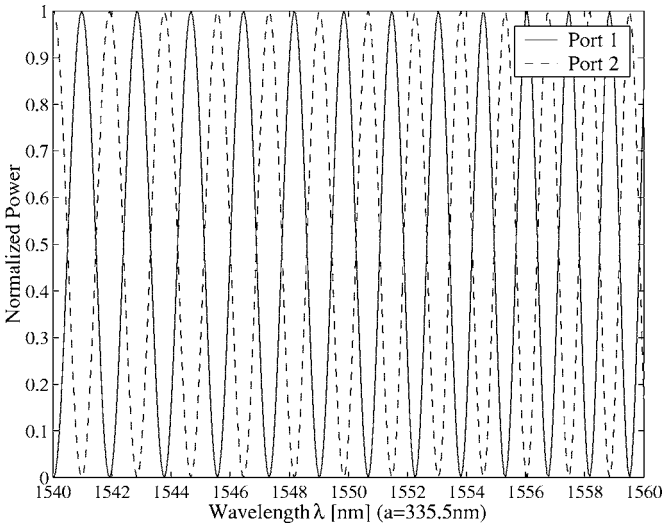

FIG. 9. Normalized power at the two output ports of coupler II for $\gamma=90°$ and $L=1400a=469.7$ μm.

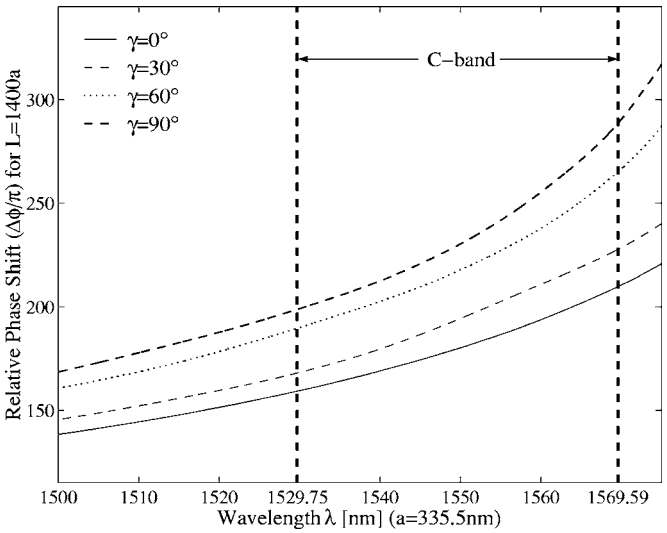

FIG. 10. Relative phase shift between the coupler II supermodes accumulated after 1400a when a=335.5 nm.

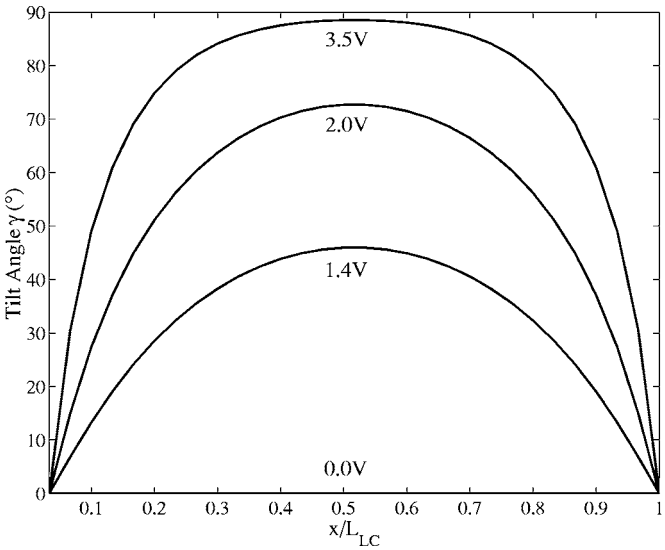

FIG. 12. Nematic director profile across the liquid crystal layer for different values of the applied voltage.

waveguides are identical and consist of a liquid crystal layer surrounded by two thin films of ITO, where electrodes are attached. In this way the properties of each waveguide and consequently the characteristics of the directional coupler can be controlled by the application of a static voltage V. The thickness of the liquid crystal and the ITO layers equals a and $a/5$, respectively. Additionally, it is assumed that appropriate surface treatment promotes strong molecular anchoring. Liquid crystals confined between parallel planar surfaces are very commonly encountered in certain practical applications, such as those related to display technology. Enforcement of strong molecular anchoring at planar surfaces is realized by various well-developed techniques, such as rubbing or photoalignment. The nematic director profile for a specific value of the applied voltage is found through a minimization technique of the total free energy per unit volume. This requires solution of the resulting Euler equation along with the zero-divergence Maxwell's equation and it is done using a finite difference method combined with a successive overrelaxation scheme. Four resulting patterns of the molecular orientation across the liquid crystal layer are illustrated in Fig. 12 for different values of the applied voltage. The considered elastic constants and the relative static permittivities of E7 are $K_{11}=K_{33}=12$ pN and $\varepsilon_{\parallel}=19.16$ and $\varepsilon_{\perp}=5.42$, respectively.

The dispersion diagram of the single isolated waveguide is presented in Fig. 13, while the supermodes of directional coupler III can be seen in the dispersion diagram of Fig. 14. In this case, two main modes for the waveguide and four supermodes for the coupler appear inside the band gap. We will focus on the two supermodes in the middle. The operational frequency regime is limited by the existence of the other supermodes to the range $0.214-0.2455(c/a)$, as marked by the dashed horizontal lines in Fig. 14. The strong tuning of the dispersion curves is evident in this case too. Unfortunately, the decoupling frequencies are not contained in this operational frequency range. Using the dispersion diagram of Fig. 14, we have derived the normalized coupling length as a function of the normalized frequency. The results are shown in Fig. 15, where it can be observed that higher coupling lengths are acquired in this case, with maximum values reported for zero voltage. It must be remarked that the coupling length does not increase even when the radii of the

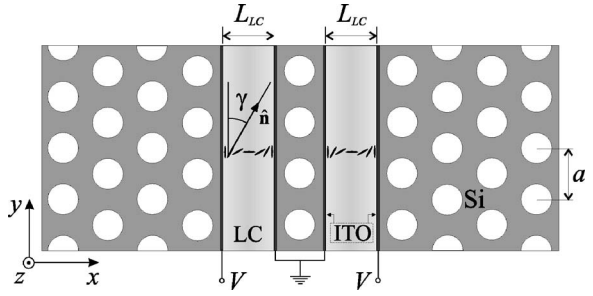

FIG. 11. Layout of directional coupler III.

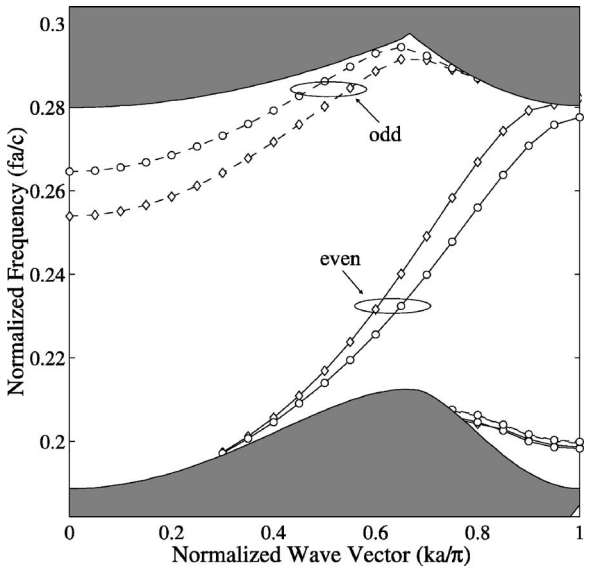

FIG. 13. Dispersion diagram for TE modes of the single isolated waveguide. Solid curves indicate even modes, and dashed curves correspond to odd modes. Diamonds: V=0 V; circles: V=3.5 V.

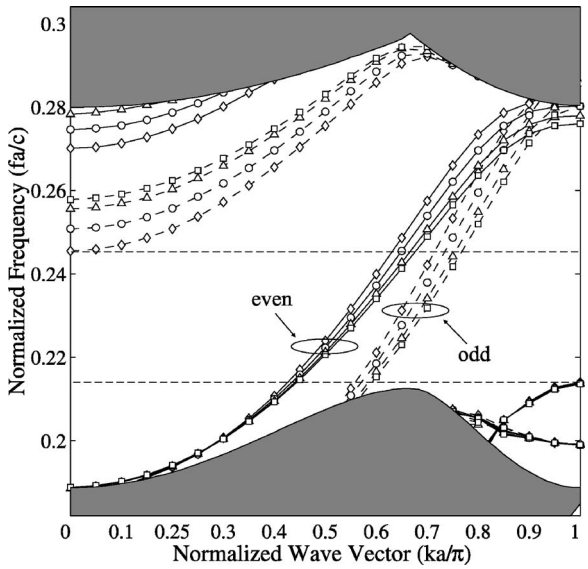

FIG. 14. Dispersion diagram for TE supermodes of directional coupler III. Solid curves indicate even modes, and dashed curves correspond to odd modes. Diamonds: $V=0$ V; circles: $V=1.4$ V; triangles: $V=2$ V; squares: $V=3.5$ V.

air rods between the waveguides are increased so that the effective permittivity of the interacting region is reduced. Instead, as the holes in the central row are made bigger, the region where only two supermodes (one of even and one of odd parity) are allowed to propagate is diminished, so that the resulting coupling length is overally augmented.

Finally, the channel interleaving operation is investigated. As in the previous instance, the coupled mode theory is utilized to find the proper overall length in order to accomplish a 0.8 nm separation between adjacent channels. The normalized output power at the two branches is illustrated in Fig. 16 for $V=3.5$ V and $a=375$ nm. Owing to small slopes of the coupling coefficient curve inside the operational frequency range, the coupler's length is found rather large, approximately $L=4500a=1.68$ mm. However, the almost constant κ slope results in equally spaced channels throughout the whole C band.

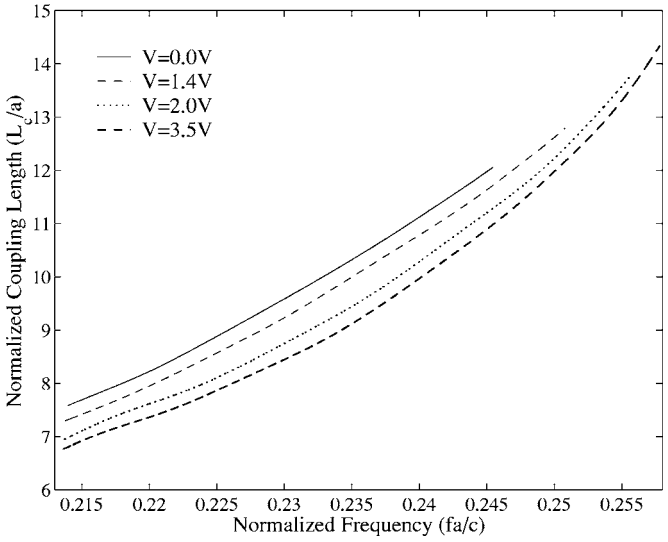

FIG. 15. Normalized coupling length of directional coupler III.

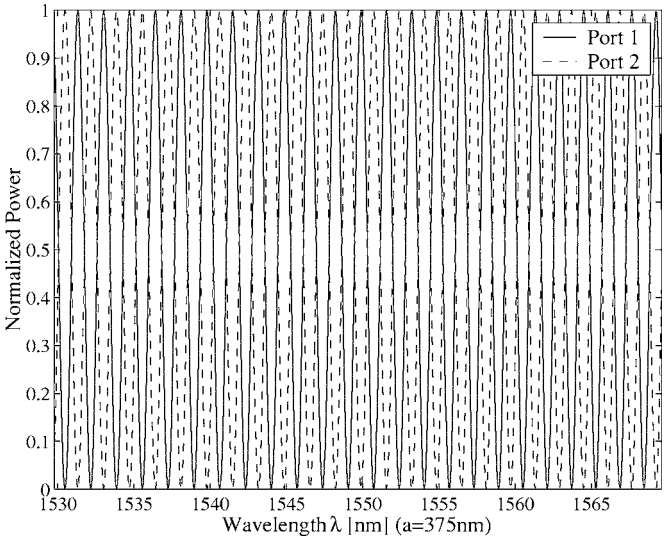

FIG. 16. Normalized power at the two output ports of coupler III for $V=3.5$ V and $L=4500a=1.68$ mm.

The results of this study have been obtained in the context of 2D calculations; however, they could be representative of directional couplers realized in low index-contrast photonic crystal slabs.[34] Such an extension would premise the use of an appropriate effective refractive index for the slab structure and would allow for a classification of the corresponding supermodes into guiding or leaky.

III. CONCLUSIONS

Two photonic crystal directional coupler structures infiltrated with a nematic liquid crystal in the waveguide region have been analyzed. It has been demonstrated that their properties strongly depend on the orientation of the liquid crystal molecules, which can be controlled by the application of an external static electric field. In the first case, where the liquid crystal is inserted into the air voids constituting the coupler branches, coupling lengths as short as $2a$ and $4a$ have been achieved in the two alternative layouts. Furthermore, the capability of these couplers to operate as channel interleavers has been thoroughly investigated. It has been revealed that a channel spacing of 0.8 nm can be achieved in the 1550 nm window with an overall length of barely 195 μm. In addition, equally separated channels with a 0.8 nm spacing can be acquired in a range covering a large portion of the C band with a device as short as 549 μm. An alternative configuration where the waveguides are made of liquid crystal layers has been also studied. In this case substantially larger device lengths are required in order to provide narrow constant channel spacings.

ACKNOWLEDGMENTS

This work was partially supported by the Greek General Secretariat of Research and Technology under Grant No. PENED/01ED27.

[1]E. Yablonovitch, Phys. Rev. Lett. **58**, 2059 (1987).
[2]J. D. Joannopoulos, R. D. Meade, and J. N. Winn, *Photonic Crystals: Molding the Flow of Light* (Princeton University Press, Princeton, NJ,

1995).
[3]I. Vorobeichic, M. Orenstein, and N. Moiseyev, IEEE J. Quantum Electron. **34**, 1772 (1998).
[4]M. Koshiba, J. Lightwave Technol. **19**, 1970 (2001).
[5]S. Boscolo, M. Midrio, and C. G. Someda, IEEE J. Quantum Electron. **38**, 47 (2002).
[6]T. Koponen, A. Huttunen, and P. Törmä, J. Appl. Phys. **96**, 4039 (2004).
[7]A. Martinez, F. Guesta, and J. Marti, IEEE Photonics Technol. Lett. **15**, 694 (2003).
[8]J. Zimmermann, M. Kamp, A. Forchel, and R. März, Opt. Commun. **230**, 387 (2004).
[9]M. Qiu and M. Swillo, Photonics Nanostruct. Fundam. Appl. **1**, 23 (2003).
[10]F. S.-S. Chien, Y.-J. Hsu, W.-F. Hsieh, and S.-C. Cheng, Opt. Express **12**, 1119 (2004).
[11]Y. Tanaka, H. Nakamura, Y. Sugimoto, N. Ikeda, K. Asakawa, and K. Inoue, IEEE J. Quantum Electron. **41**, 76 (2005).
[12]M. Thorhauger, L. H. Frandsen, and P. I. Borel, Opt. Lett. **28**, 1525 (2003).
[13]T. P. White, L. C. Botten, R. C. McPhedran, and C. Martijn de Sterke, Opt. Lett. **28**, 2452 (2003).
[14]I. Park, H.-S. Lee, H.-J. Kim, K.-M. Moon, S.-G. Lee, B.-H. O, S.-G. Park, and E.-H. Lee, Opt. Express **12**, 3599 (2004).
[15]S. Chandrasekhar, *Liquid Crystals* (Cambridge University Press, Cambridge, 1995).
[16]F. Guesta-Soto, A. Martinez, J. Garcia, F. Ramos, P. Sanchis, J. Blasco, and J. Marti, Opt. Express **12**, 161 (2004).
[17]A. Locatelli, D. Modotto, D. Paloschi, and C. De Angelis, Opt. Commun. **237**, 97 (2004).
[18]E. P. Kosmidou, E. E. Kriezis, and T. D. Tsiboukis, IEEE J. Quantum Electron. **41**, 657 (2005).
[19]R. Ozaki, T. Matsui, M. Ozaki, and K. Yoshino, Appl. Phys. Lett. **82**, 3593 (2003).
[20]H. Ozaki and K. Yoshino, Phys. Rev. B **67**, 073106 (2003).
[21]C.-T. Kuo, S.-Y. Huang, I.-M. Jiang, and M.-S. Tsai, J. Appl. Phys. **97**, 103113 (2005).
[22]T. Yasuda, Y. Tsuji, and M. Koshiba, IEEE Photonics Technol. Lett. **17**, 55 (2005).
[23]C.-Y. Liu and L.-W. Chen, IEEE Photonics Technol. Lett. **16**, 1849 (2004).
[24]E. E. Kriezis and S. J. Elston, Opt. Commun. **177**, 69 (2000).
[25]C. V. Brown, E. E. Kriezis, and S. J. Elston, J. Appl. Phys. **91**, 3495 (2002).
[26]C. T. Chan, Q. L. Yu, and K. M. Ho, Phys. Rev. B **51**, 16635 (1995).
[27]A. P. Zhao, IEEE Trans. Microwave Theory Tech. **46**, 1511 (1998).
[28]E. P. Kosmidou, T. I. Kosmanis, and T. D. Tsiboukis, IEEE Trans. Magn. **39**, 1191 (2003).
[29]Y. Huang, Y. Xu, and A. Yariv, Appl. Phys. Lett. **85**, 5182 (2004).
[30]S. V. Burylov, JETP **85**, 873 (1997).
[31]J. Martz, B. Wild, R. Ferrini, L. A. Dunbar, M. Mulot, S. Anand, R. Houdré, and L. Zuppiroli, Proc. SPIE **5926**, 1 (2005).
[32]E. P. Kosmidou and E. E. Kriezis, Proc. SPIE **6182**, 215 (2006).
[33]A. Yariv, IEEE J. Quantum Electron. **9**, 919 (1973).
[34]M. Qiu, Appl. Phys. Lett. **81**, 1163 (2002).